AGU PUBLICATIONS

JGR

Journal of Geophysical Research: Space Physics

RESEARCH ARTICLE
10.1002/2014JA020939

Key Points:
- Pickup ion distributions are simulated in a model CIR
- Pickup ions have different cooling behavior in the compression and rarefaction region
- Pickup ions are accelerated in the compression region of the model CIR

Correspondence to:
N. A. Schwadron,
nschwadron@guero.sr.unh.edu

Citation:
Chen, J. H., N. A. Schwadron, E. Möbius, and M. Gorby (2015), Modeling interstellar pickup ion distributions in corotating interaction regions inside 1 AU, *J. Geophys. Res. Space Physics*, *120*, 9269–9280, doi:10.1002/2014JA020939.

Received 10 DEC 2014
Accepted 17 SEP 2015
Accepted article online 22 SEP 2015
Published online 27 NOV 2015

Modeling interstellar pickup ion distributions in corotating interaction regions inside 1 AU

J. H. Chen[1], N. A. Schwadron[1], E. Möbius[1], and M. Gorby[1]

[1]Space Science Center and Department of Physics, University of New Hampshire, Durham, New Hampshire, USA

Abstract We present a modeling study of interstellar pickup ion (PUI) distributions in corotating interaction regions (CIRs). We consider gradual compressions associated with CIRs formed when fast speed streams overtake slower streams in the inner heliosphere. For the analysis, we adopt a simplified magnetohydrodynamic model of a CIR. The Energetic Particle Radiation Environment Module, a parallelized particle numerical kinetic code, is used to model PUI distributions using the focused transport equation, including adiabatic cooling/heating, adiabatic focusing, and parallel and perpendicular diffusion. The continuous injection of PUIs is handled as a source term with a ring distribution in velocity space that is produced from the local neutral density obtained from a hot model of the interstellar neutral gas. The simulated distributions exhibit a harder spectrum in the compression region and a softer spectrum in the rarefaction region than that in undisturbed solar wind. As an additional result, a v^{-5} power law tail distribution above the PUI cutoff speed (a knee in the distribution) emerges for a particular velocity gradient in the CIR. The tail above the PUI cutoff is sensitive to the CIR velocity gradient, and in one observational case studied, this relationship adequately explains the observed spectrum from 2 to 4 times the solar wind speed. This suggests that the velocity gradient associated with the CIR formation can efficiently create a seed population of PUIs before a shock forms even without stochastic acceleration. Thus, local CIR compressions without shocks may play a significant role in the acceleration process as suggested previously.

1. Introduction

Interstellar gas penetrates into the inner heliosphere as a neutral wind due to the relative motion between the Sun and the local interstellar medium (LISM). When approaching the Sun, the interstellar neutral gas is gradually ionized by photoionization, by charge exchange with solar wind protons and alpha particles, and also by solar wind electrons to an increasing fraction closer to the Sun. As a consequence, these newly generated ions are immediately picked up by the interplanetary magnetic field and convected outward with the solar wind. These ions constitute a distinct charged particle distribution referred to as interstellar pickup ions (PUIs) [*Möbius et al.*, 1985; *Gloeckler et al.,* 1993; *Geiss et al.,* 1994]. Interstellar PUIs have been widely studied over the last three decades for three important reasons: First, interstellar PUIs are an excellent tool for the study of the physical parameters and composition of the LISM. Second, interstellar PUIs provide important information on the propagation of low-rigidity energetic particles. Additionally, interstellar PUIs have been identified as important source particles for effective acceleration at compressions and shocks due to their very nonthermal velocity distribution.

Due to the combined influence of ionization and the Sun's gravitational force on the interstellar neutral gas, a characteristic focusing cone centered on the flow direction is formed on the downwind side of the Sun (for all species except H). Helium is almost unaffected at the heliospheric interface because of its weak charge exchange interaction and thus provides us with almost completely unbiased information about the physical parameters of LISM. He^+ PUI observations on the downwind side provide us with a useful tool to determine the physical parameters of interstellar neutral He gas [e.g., *Möbius et al.,* 1995; *Gloeckler et al.,* 2004]. However, the strong variation of PUI fluxes and distributions impact the cone observations and limit the accuracy of studies because solar activity, interplanetary parameters, and large-scale solar wind structure strongly affect PUI generation and transport. For example, the maximum PUI flux varies with the typical ionization rate over a solar cycle. In addition, the anisotropic PUI velocity distributions can lead to broadening and positional shift in the ecliptic plane of the focusing cone as observed in the PUIs [*Möbius et al.,* 1995]. In the case of quasi-radial interplanetary magnetic field and low level of magnetic turbulence, the PUI velocity distribution is anisotropic and the bulk of the PUIs moves sunward along the magnetic field lines in the solar wind frame. This particle

streaming effect may lead to broadening and a longitudinal shift of the cone-induced PUI feature [e.g., *Chalov and Fahr,* 1999]. Furthermore, enormous compressions of the PUI distributions in corotating interaction regions (CIR) with enhanced ionization (e.g., charge exchange and electron impact ionization) and high level of magnetic turbulence lead to a substantial substructure superimposed on the PUI cone. A correlation between PUI flux and solar wind flux due to compressions and rarefactions is observed [*Möbius et al.,* 2010], but still with substantial additional variations of unknown origin.

The interstellar neutral gas distribution can be mapped into the PUI velocity distribution, using the adiabatic cooling equation $(v/U)^{\alpha} = (r/r_0)$ with α defined as adiabatic cooling index. v, U, r, and r_0 are the PUI speed at the observer location, the solar wind speed, the location of the generation of the PUIs, and the observer location, respectively. *Chen et al.* [2013] have shown that the adiabatic cooling index varies with solar activity between ~1 and 2, compared with a constant value of 1.5 as assumed previously [*Vasyliunas and Siscoe,* 1976]. They argued that potential contributors to these variations might be solar wind compression and rarefaction regions and enhancements of the electron ionization rate in solar wind compressions, which is the only ionization process that does not scale a $1/r^2$. In a recent study *Chen et al.* [2014] showed that variations in the electron ionization rate have a negligible influence on PUI distributions, even in strong compression regions. This leaves the different radial expansion behavior of solar wind compression and rarefaction regions as the most likely candidate for the observed variations in the PUI cooling. This suggestion appears to dovetail with the observed strong variations of PUI fluxes across the focusing cone.

On the other hand, the observation of PUIs in the inner heliosphere has revealed the ubiquitous presence of the pronounced suprathermal tails with a spectral index of -5 above the cutoff speed of PUI velocity distributions [*Gloeckler*, 2003; *Fisk and Gloeckler,* 2006, 2007, 2008]. This suprathermal tail may result from particles undergoing stochastic acceleration in compressional turbulence [*Fisk and Gloeckler,* 2006], which is formed by a cascade in energy analogous to the turbulence cascade [*Kolmogorov*, 1941]. These suprathermal particles may be further accelerated by forward and reverse shocks, which surround CIRs between ~2 and 5 AU, via diffusive shock acceleration, and then propagate sunward along magnetic field lines [*Fisk and Lee,* 1980]. More recently, *Desai et al.* [1999] have shown that standard diffusive shock acceleration cannot explain the observed energetic protons at CIR shocks. Conversely, *Chalov* [2001] has shown that acceleration of pickup protons at forward and reverse shocks can be explained by shock drift acceleration. Observations of CIR associated energetic particles also suggest that they may even be accelerated within CIR compression regions without the presence of shocks [e.g., *Mason*, 2000; *Chotoo et al.,* 2000; *Ebert et al.,* 2012]. For this reason, *Giacalone et al.* [2002] suggested that low-energy particles could be accelerated in regions of gradual solar wind compression, such as CIRs near 1 AU where forward and reverse shocks are not formed yet. In their mechanism, particles gain energy through repeatedly sampling the solar wind speed gradient across the compression in a process similar to diffusive shock acceleration at a quasi-parallel shock.

In this study, we will employ a similar model of a CIR in the solar wind to study the interstellar helium PUI propagation in the solar wind compression and rarefaction regions. Our simulation results show enhanced cooling in the compression region and a reduction in the rarefaction region. The cooling rate is determined by the gradient of the solar wind speed. In addition, the PUI distribution averaged over the compression region exhibits a high-energy tail distribution above the PUI cutoff speed, which provides further evidence that some particles of this population are accelerated locally in the CIR compression regions even in the absence of shocks.

2. Magnetohydrodynamic Model of a CIR

The starting point for the simulation of the PUI distributions is the modeling of solar wind speed, density, and interplanetary magnetic field in a CIR. Here we take a simple model of a CIR constructed by *Giacalone et al.* [2002], which is applicable for heliocentric distances ≤ 2 AU where the forward and reverse shocks have not yet formed. From this model, the radial solar wind flow speed is taken as U in the nonrotating heliocentric frame. In a frame corotating with the Sun at rate Ω_s, the flow velocity, U_c, has components in both the radial and the azimuthal directions, where the azimuthal flow speed can be written as $-\Omega_s r \sin\theta$ with θ defined as the colatitude. We are using spherical coordinates, r, ϕ, and θ, which are defined in the corotating frame. The radial component U is assumed to be a function of radial distance r, and azimuthal angle ϕ:

$$U(r,\phi) = U_s + \frac{1}{2}(U_f - U_s)\tanh\left(\frac{\phi_c - \Omega_s r/W - \phi}{\Delta\phi_c}\right) - \frac{1}{2}(U_f - U_s)\tanh\left(\frac{\phi_{rf} - \Omega_s r/W - \phi}{\Delta\phi_{rf}}\right) \quad (1)$$

where U_s and U_f are the slow and fast solar wind speeds, respectively. The angular parameters $\{\phi_c, \Delta\phi_c\}$ and $\{\phi_{rf}, \Delta\phi_{rf}\}$ specify the location and azimuthal width of the compression and subsequent rarefaction regions. The parameter W is the speed of the disturbance, moving radially outward in the nonrotating heliocentric frame. Therefore, this model may reproduce either a "reverse" (W is slower than the slow solar wind speed, U_s) or a "forward" (W is faster than the fast solar wind speed, U_f) compression in the solar wind. The width of the compression region along a specific radial vector can be simply given by $\Delta_c = W\Delta\phi_c/\Omega_s$.

In order to obtain the density $\rho(r, \phi)$, we invoke the continuity equation in the corotating frame

$$\nabla \cdot \left(\rho \vec{U_c}\right) = 0 \tag{2}$$

which is expressed in spherical coordinates

$$\frac{\partial}{\partial r}\left(r^2 \rho U\right) - \frac{\partial}{\partial \phi}\left(r^2 \rho W\right)\left(\frac{\Omega_s}{W}\right) = 0 \tag{3}$$

It is readily shown that the gradient of the solar wind speed $U(r, \phi)$ obeys

$$\frac{\partial U}{\partial r} - \frac{\partial U}{\partial \phi}\left(\frac{\Omega_s}{W}\right) = 0 \tag{4}$$

By comparison of equation (3) with equation (4), $r^2\rho U$ and $r^2\rho W$ can be introduced as

$$r^2 \rho U = Cf(U) + C_1 \tag{5a}$$

$$r^2 \rho W = Cf(U) + C_2 \tag{5b}$$

where C, C_1, and C_2 are constant, and $f(U)$ is a function of solar wind speed U. By subtracting equation (5b) from equation (5a), we obtain

$$r^2 \rho U - r^2 \rho W = C_1 - C_2 \tag{6}$$

Here $C_1 - C_2$ can be used to fit the boundary condition on the surface of the Sun. We assume that the slow solar wind density at the surface of the Sun $r = r_s$ is ρ_s, thus, $C_1 - C_2$ satisfies

$$C_1 - C_2 = \rho_s r_s^2 (U_s - W) \tag{7}$$

Substituting equation (7) into (6) yields

$$\rho(r, \phi) = \rho_s \frac{U_s - W}{U(r, \phi) - W}\left(\frac{r_s}{r}\right)^2 \tag{8}$$

[See *Giacalone et al.,* 2002, equation (5)].

A divergence-free magnetic field is introduced to be parallel to the solar wind velocity in the corotating frame:

$$\vec{B} = \Psi_i \rho \vec{U_c} \tag{9}$$

In this case, the magnetic field is of the following form [*Giacalone et al.,* 2002; *Kocharov et al.,* 2003]:

$$B_r(r, \phi) = \frac{\Psi_i}{U(r, \phi) - W}\left(\frac{r_s}{r}\right)^2 U(r, \phi) \tag{10a}$$

$$B_\phi(r, \phi) = -\frac{\Psi_i}{U(r, \phi) - W}\left(\frac{r_s}{r}\right)^2 \Omega_s r \sin\theta \tag{10b}$$

where Ψ_i is the normalization factor for a magnetic field line "i". Ψ_i is deduced from the boundary condition that the magnetic field strength at the foot point (r_s, ϕ_i) of this magnetic field line is equal to the boundary value $B(r_s, \phi_i)$. Hence, the nearly radial magnetic field near the Sun leads Ψ_i to

$$\Psi_i \approx (U(r_s, \phi_i) - W)\frac{B_r(r_s, \phi_i)}{U(r_s, \phi_i)} \tag{11}$$

Here we use a uniform boundary field $B_r(r_s, \phi_i) = 1G$ to compute the magnetic field based on equation (10a) and (10b). Throughout the paper, we adopt the following values for the angular parameters of the CIR: $\Delta\phi_c = 1^0$, $\Delta\phi_{rf} = 25^0$, and $\phi_c - \phi_{rf} = 70^0$. Note, to avoid a singularity in equation (8) W must be smaller (for a reverse

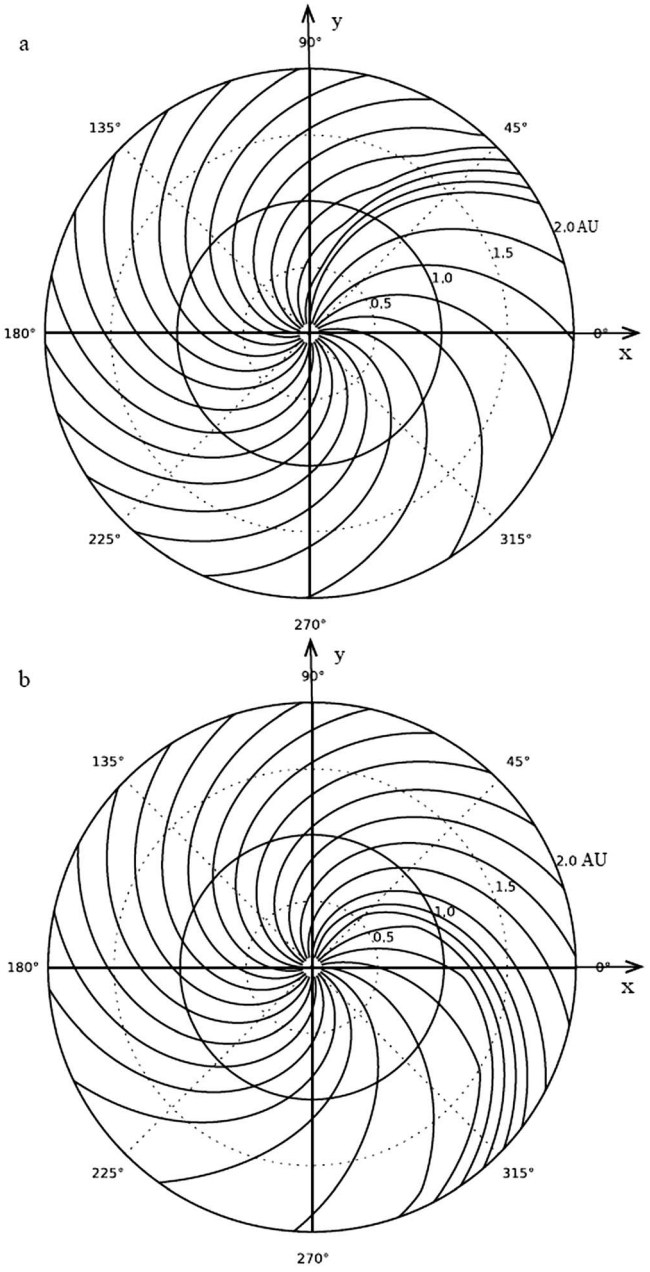

Figure 1. Magnetic field lines on the ecliptic plane inside 2 AU. The parameters are $\Delta\phi_c = 1^0$, $\Delta\phi_{rf} = 25^0$, $\phi_c - \phi_{rf} = 70^0$, $U_f = 800$ km/s, and $U_s = 400$ km/s. (a) Forward compression with $W = 1200$ km/s. (b) Reverse compression with $W = 300$ km/s.

compression) or larger (for a forward compression) than $U(r, \phi)$ everywhere. The magnetic field configurations are shown in Figure 1.

3. Kinetic Model of PUIs and Suprathermal Particles

Two main theoretical approaches are used to describe charged particle (e.g., PUIs, suprathermal, and energetic particles) transport in collisionless tenuous interplanetary magnetized plasmas, namely, a diffusive transport equation or a focused transport equation. The diffusive approximation assumes that the particle velocity distribution function adjusts very rapidly to quasi-equilibrium through pitch angle diffusion, which limits the model to nearly isotropic distributions. This approach can be described by Parker's equation [*Parker*, 1965], which includes the effects of spatial diffusion, drifts, convection, and adiabatic cooling. It is widely used to describe the transport of anomalous cosmic rays, galactic cosmic rays, and solar energetic particle events, including diffusive shock acceleration of energetic particles. However, it has been pointed out that the diffusive approximation should not be applied to model particle transport if the scattering of particles is weak. This is because weak scattering leads to strong anisotropies in the particle distribution function. A better treatment for these conditions is provided by a focused transport model [e.g., *Roelof*, 1969; *Ruffolo*, 1995; *Kóta et al.,* 2005], which describes particle scattering on a more elementary level. The focused transport equation has a broader range of validity and can cover large anisotropies as well as low-energy particle distributions. Under these circumstances, the spatial diffusion concept is replaced by the consideration of pitch angle and energy diffusion processes so that the particle distribution is not necessarily isotropic.

In order to compute the PUI velocity distributions in structured solar wind, we use the Energetic Particle Radiation Environment Module (EPREM) [*Schwadron et al.,* 2010], a highly versatile and flexible parallelized numerical kinetic particle code that accounts for the time-dependent transport of PUIs, suprathermal, and energetic particles along and across magnetic field lines for any field and flow topology in three dimensions. It produces time histories of the particle velocity distribution functions as a function of pitch angle and energy, appropriate for the magnetohydrodynamic (MHD) conditions in the heliosphere. The transport of

particles parallel to the interplanetary magnetic field is treated in the EPREM model with a focused transport equation. Along each field line, EPREM solves for particle streaming, adiabatic focusing and cooling, convection, pitch angle scattering, and stochastic acceleration, using the *Kóta et al.* [2005] formalism. A slightly modified form of the focused transport equation [*Skilling*, 1971; *Ruffolo*, 1995] is used to treat transport and energy change:

$$\begin{aligned}
&\left(1-\frac{\vec{V}\cdot\vec{e_b}\,v\mu}{c^2}\right)\frac{\mathrm{d}f}{\mathrm{d}t} && \text{(convection)}\\
&+v\mu\,\vec{e_b}\cdot\nabla f && \text{(streaming)}\\
&+\frac{(1-\mu^2)}{2}\left[-v\,\vec{e_b}\,\nabla\ln B-\frac{2}{v}\vec{e_b}\cdot\frac{\mathrm{d}\vec{V}}{\mathrm{d}t}+\mu\frac{d\ln\left(n^2/B^3\right)}{\mathrm{d}t}\right]\frac{\partial f}{\partial\mu} && \text{(adiabatic focusing)}\\
&+\left[-\frac{\mu\,\vec{e_b}}{v}\cdot\frac{\mathrm{d}\vec{V}}{\mathrm{d}t}+\mu^2\frac{d\ln(n/B)}{\mathrm{d}t}+\frac{(1-\mu^2)d\ln B}{2\quad\mathrm{d}t}\right]\frac{\partial f}{\partial\ln p} && \text{(adiabatic cooling/heating)}\\
&=\frac{\partial}{\partial\mu}\left(\frac{D_{\mu\mu}\partial f}{2\ \partial\mu}\right) && \text{(pitch angle scattering)}\\
&-\frac{1}{p^2}\frac{\partial}{\partial p}\left(p^2D_{pp}\frac{\partial f_0}{\partial p}\right) && \text{(stochastic acceleration)}\\
&+Q
\end{aligned} \tag{12}$$

Here the notation, $\frac{d}{\mathrm{d}t}$ stands for the convective derivative, i.e., $\frac{d}{\mathrm{d}t}=\frac{\partial}{\mathrm{d}t}+\vec{V}\cdot\nabla$, $\vec{V}$ is the solar wind flow velocity, $\vec{e_b}$ is the unit vector along the magnetic field, μ is the cosine of the pitch angle, n is the solar wind density, B is the magnetic field strength, p is the particle momentum, v is the particle speed, and Q is the particle source term. f is the particle velocity distribution, and $f_0=\frac{1}{2}\int_{-1}^{1}f(t,x,v,\mu)d\mu$ is isotropic portion of the distribution function. The pitch angle diffusion coefficient is given by [*Isenberg*, 1997; *Schwadron*, 1998; *Kóta*, 2000]

$$D_{\mu\mu}=\frac{(1-\mu^2)v}{2\lambda_p} \tag{13}$$

where λ_p is the parallel mean free path and has the form [e.g., *Erdõs*, 1999; *Sakai*, 2002; *Chollet et al.,* 2010]

$$\lambda_p=\lambda_0\left(\frac{r}{1\ \mathrm{AU}}\right)^{2/3} \tag{14}$$

λ_0 is the parallel mean free path at 1 AU, p is the particle momentum, c is the speed of light, and r is the radial distance in astronomical unit. D_{pp} is associated with diffusion in particle momentum. In the modeling presented here, we neglect stochastic acceleration and perpendicular diffusion. The advantage of the formulation in equation (12) is that most of the transport coefficients are obtained simply by differencing the bulk plasma quantities (e.g., density, field strength, and plasma velocity) at each "node" moving with the solar wind flow from the values at the previous time step to the updated values.

In addition to solving for the parallel transport, perpendicular transport can be solved for within EPREM by a separate solver for cross-field diffusion and particle drift. However, in our simulation, we turned perpendicular transport and drift off.

Interstellar PUIs are charged particles injected from a well-defined source, e.g., interstellar neutral gas, by ionization. The spatial distribution of interstellar neutral helium is calculated on the basis of a hot interstellar gas model [*Fahr,* 1971; *Thomas,* 1978; *Wu and Judge,* 1979], which takes the finite LISM temperature of helium into account. Helium atoms penetrate deeply into inner heliosphere and, when passing through the solar gravity field, form a strongly pronounced density increase, i.e., the helium focusing cone, along the downwind direction. They also suffer losses along their hyperbolic trajectory due to ionization processes. Here we assume that the loss of the neutral helium atoms and the production of PUIs are only due to photoionization, which is very reasonable because of the negligible effect of charge exchange ionization for helium atoms. In addition, *Chen et al.* [2014] found that electron impact ionization has negligible effect on the shape of helium PUI velocity distribution. After their ionization, PUIs are injected at each "node" continuously as a ring distribution in velocity space, centered on the local magnetic field line. To model the helium neutral gas distribution and PUI production, we

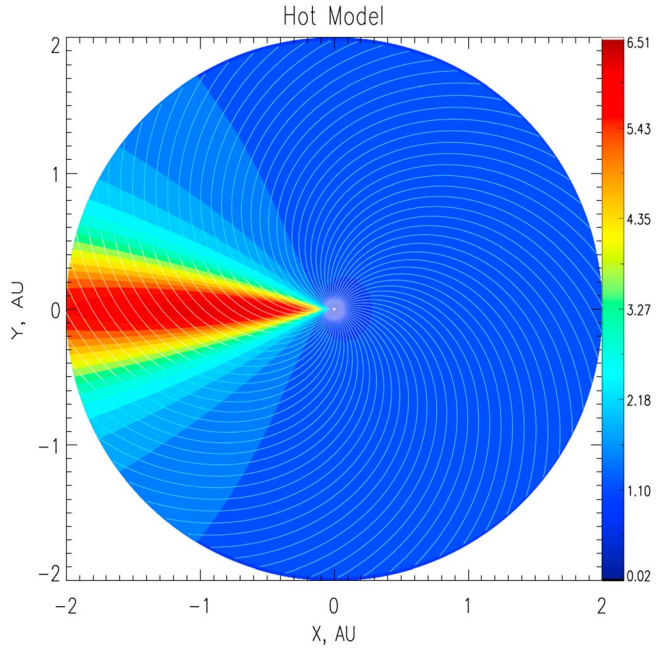

Figure 2. Hot model distributions of the number density of interstellar neutral helium normalized to $n_{He} = 0.015\ cm^{-3}$. The *X* axis corresponds to interstellar neutral gas inflow direction. A helium density focusing cone is formed in the downwind direction. The white lines are the Parker spiral magnetic field lines.

take the helium temperature, density, and bulk speed in the LISM as $T_\infty = 6300$ K, $n_{He} = 0/015\ cm^{-3}$, and $V_\infty = 23.2$ km/s . While there is an ongoing as to the best combination of interstellar flow speed and direction [*Bzowski et al.*, 2012; *Möbius et al.*, 2012; *Vincent et al.*, 2014; *Katushkina et al.*, 2014; *Bzowski et al.*, 2014; *Lallement & Bertaux*, 2014, *McComas et al.*, 2015; *Leonard et al.*, 2015]. The potential difference in the speed between 23 and 26 km/s has a negligible effect on our results. We take the helium atom loss rate and PUI production rate at 1 AU as $\beta_0^+ = 7.5\times10^{-8}\ s^{-1}$ and $\beta_0^- = 7.5\times 10^{-8}\ s^{-1}$. Figure 2 shows the number density of the interstellar helium within the heliosphere for the hot gas model, overlaid with Parker spiral magnetic field lines.

Previously, EPREM has been applied to study helium PUIs (0.5–10 keV) [*Hill et al.*, 2009] and relatively low-energy solar energetic particle (SEP) events (1–500 MeV) [e.g., *Dayeh et al.*, 2010]. Before diving into the detailed study of PUI evolution, we have verified and validated the EPREM model for PUIs in comparison with the analytic solutions based on *Vasyliunas and Siscoe* [1976]. Here we have used a constant solar wind speed of 450 km/s, a Parker spiral magnetic field with a value of 5 nT, and a parallel scattering mean free path for He^+ PUIs of 0.1 AU at 1 AU. Note that perpendicular transport and stochastic acceleration are turned off, and PUIs only propagate along individual field lines. An example of a validation run is shown in Figure 3. Along the upwind direction, the simulated He^+ PUI velocity distribution mimics closely the analytic solution according to *Vasyliunas and Siscoe* [1976], which indicates that EPREM works very well for the relatively low-energy PUIs. The differences at low PUI speed can be traced to issues related to numerical diffusion on vanishingly small energy cell sizes. However, for the accumulation of PUIs along the focusing cone there are substantial differences that can be traced to realistic kinetic effects, starting immediately below solar wind speed, which result from the large azimuthal gradients in the PUI source distribution. The analytic solution of *Vasyliunas and Siscoe* [1976], in which PUIs are assumed to simply convect radially with the solar wind as an entity, provides a mapping of the neutral gas distribution exactly along the peak of focusing cone. Under these circumstances, the analytic solution does not reflect properly the actual PUI transport along magnetic field lines. More realistically, EPREM collects PUIs from left and right of the cone center along the magnetic field lines, thus reducing the effective phase space density. Therefore, EPREM, which treats kinetically the complex diffusion-convection processes of charged particles, naturally provides insight into the PUI evolution in regions with a highly variable source distribution. However, we will not address this problem further in this paper, we will rather concentrate on the PUI distributions in the structured solar wind of a CIR.

4. PUI Distribution in a Model CIR

As an illustrative example, we are modeling PUI propagation in solar wind of a CIR structure, as shown in Figure 1b. It contains a reverse compression with parameters $U_f = 800$ km/s, $U_s = 400$ km/s, and $W = 300$ km/s . We take an energy range between 10 eV and 1 MeV with an energy grid subdivided into 100 logarithmically spaced steps. The inner boundary of PUI injection is set at 0.008 AU. PUI velocity distributions along individual magnetic field lines (herein 64 field lines) are directly solved for by EPREM in the

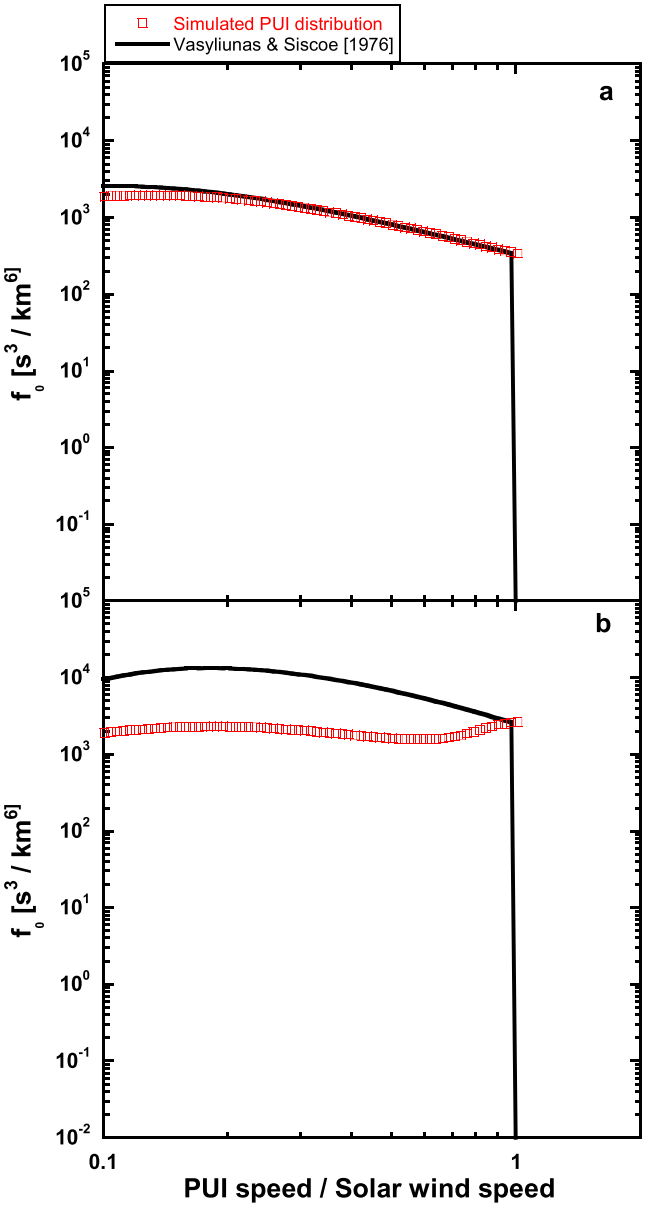

Figure 3. Comparison between simulated velocity distributions from EPREM (red) and the analytic models of *Vasyliunas and Siscoe* [1976] (black) for (a) upwind and (b) downwind, respectively. f_0 is the isotropic part of the distribution.

corotating frame following the evolving field lines. The magnetic field line structure is shown in Figure 4 (top). In the corotating frame the structure is static, while a near-Earth spacecraft orbits the sun at 1 AU over a 27 day period. Then the predicted PUI velocity distributions in the structured solar wind are the averaged distributions over the time period when the spacecraft passes through the structures. However, the effects of varying transport parameters on the result will be not discussed in this study, the comprehensive parameter study will be left to the future. Here we will concentrate on the PUI cooling behavior in the compression and rarefaction region, and possible further acceleration of PUIs in the compression region.

Shown in Figure 4 (bottom) are the He^+ PUI velocity distribution functions obtained with EPREM in the undisturbed slow wind, compression region, and rarefaction region. The distributions are computed at 1 AU in the corotating frame and averaged over ϕ/Ω_s with structural boundaries as integration limits corresponding to a spacecraft passing through the structure. In the undisturbed solar wind before the compression region, the analytic solution of *Vasyliunas and Siscoe* [1976] is again reproduced as can be expected based on the comparison of PUI distributions for the homogeneous solar wind in Figure 3. PUIs undergo adiabatic cooling as they are moving along the expanding magnetic field. For a nearly isotropic velocity distribution in the frame of solar wind equation (12) can be written as

$$2V\left(\frac{\partial f}{\partial r}-\frac{2v}{3r}\frac{\partial f}{\partial v}\right)=\int_{-1}^{1}\beta_0^+\left(\frac{r_0}{r}\right)^2 n_{\mathrm{He}}(r,\theta')\frac{\delta(v-V)\delta(\mu-\mu_0)}{2\pi V^2}\mathrm{d}\mu$$
or
$$V\left(\frac{\partial f}{\partial r}-\frac{2v}{3r}\frac{\partial f}{\partial v}\right)=\beta_0^+\left(\frac{r_0}{r}\right)^2 n_{\mathrm{He}}(r,\theta')\frac{\delta(v-V)}{4\pi V^2} \quad (17)$$

where r_0 is the location of an observer, $n_{\mathrm{He}}(r,\theta')$ is the helium density, θ' is the angle relative to the helium inflow direction, δ is the delta function, and μ_0 is the initial pitch angle at injection of the PUIs. Under the variable transformation, $w=v/V$, and $y=(r/r_0)w^{3/2}$ [*Schwadron et al.*, 2000], the transport equation (17) can be written as

$$\frac{\partial f(w,y)}{\partial w}=-3r_0 w^{\frac{1/2^{1/20}}{8ryV^4}}\beta_0^+ n_{\mathrm{He}}(r_s(w,y),\theta')\delta(w-1) \quad (18)$$

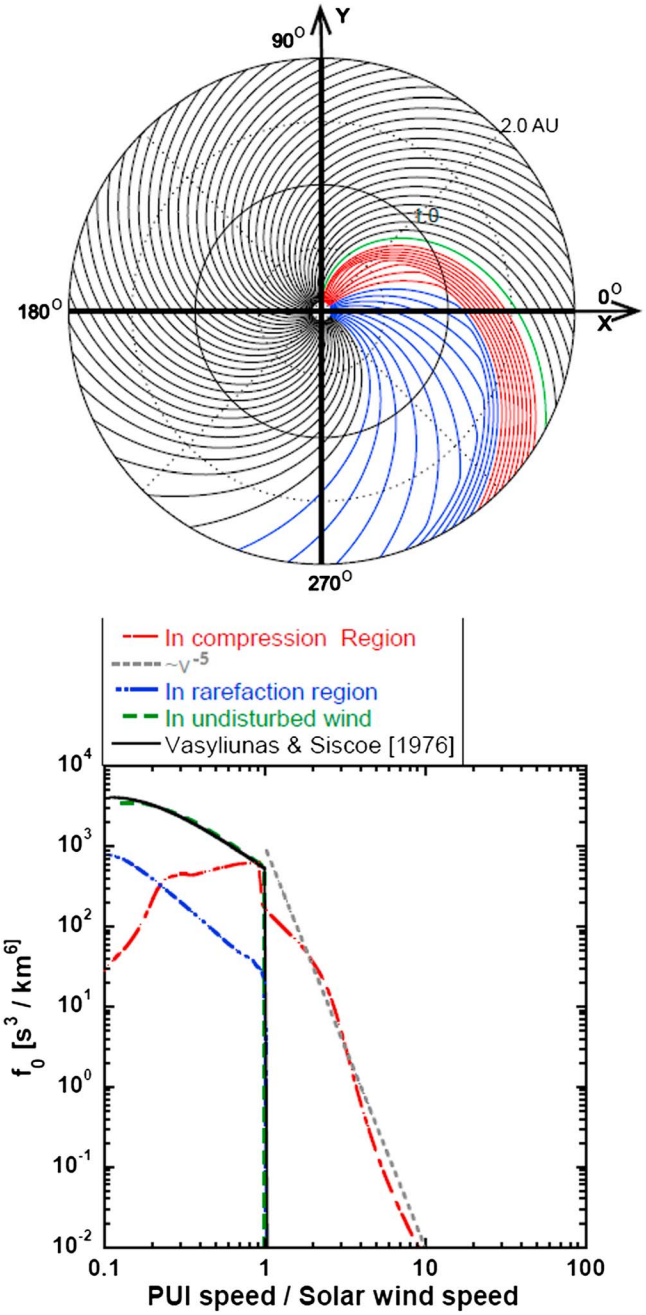

Figure 4. (top) The simulated interplanetary magnetic field lines, with the regions colored according to the spectral shown above. (bottom) PUI distributions for the compression (red) and rarefaction (blue) region of a CIR, as simulated with EPREM. A distribution in the undisturbed solar wind is also shown (green) in comparison with the analytic solution of *Vasyliunas and Siscoe* [1976] (black). A distribution that fall off as v^{-5} is shown for comparison in grey.

where the streaming variables are given by $r_s(w,y) = r_0 y w^{-3/2}$. Then the analytic solution follows:

$$f(w,r) = \frac{3r_0^2}{8\pi V^4 r'(w)} n_{\mathrm{He}}(r'(w),\theta') \quad (19)$$

where $r'(w) = rw^{3/2} = \text{const}$. Therefore, for a steady state spherically symmetric solar wind we have

$$\left(v/V\right)^{3/2} = \left(r/r_0\right) \quad (20)$$

However, the solar wind speed increases along the magnetic field lines in the rarefaction region and thus leads to a steeper distribution. Consequently, the positive gradient of the solar wind speed leads to a stronger cooling than that in the undisturbed solar wind and accordingly results in a steeper slope. In contrast to the rarefaction region, the shape of the spectrum below the PUI cutoff speed is much flatter in the compression region due to the negative gradient of solar wind speed, where PUIs undergo weaker cooling.

In addition, a power law tail distribution above the PUI cutoff speed suddenly emerges, where PUIs are accelerated to substantially higher energies than in the PUI distribution. Possible sources for acceleration are shocks, magnetic turbulence, and compressions. However, there are no shocks in the simulation, and stochastic acceleration is turned off as well. Hence, this observation of significant acceleration suggests that the negative divergence of the solar wind speed associated with the CIR formation can efficiently accelerate particles, even without a shock, as already discussed by *Giacalone et al.* [2002]. There is also a very weak tail of the distribution in the rarefaction due to the connection of the magnetic field in the rarefaction region to the compression region. However, the relevant magnitude is below ~10^{-6}, and thus insignificant.

Overall, a high-energy tail distribution in the solar wind frame is found. This tail distribution, although not a perfect power law fit, is close to the reference spectrum in Figure 4 with a -5 power law index, which indicates that compressive diffusion acceleration maybe a solution, at least under some circumstances, for the frequently observed $f(v) \sim v^{-5}$ suprathermal tail distribution [*Gloeckler et al.*, 2003; *Fisk and Gloeckler,* 2006, 2007, 2008].

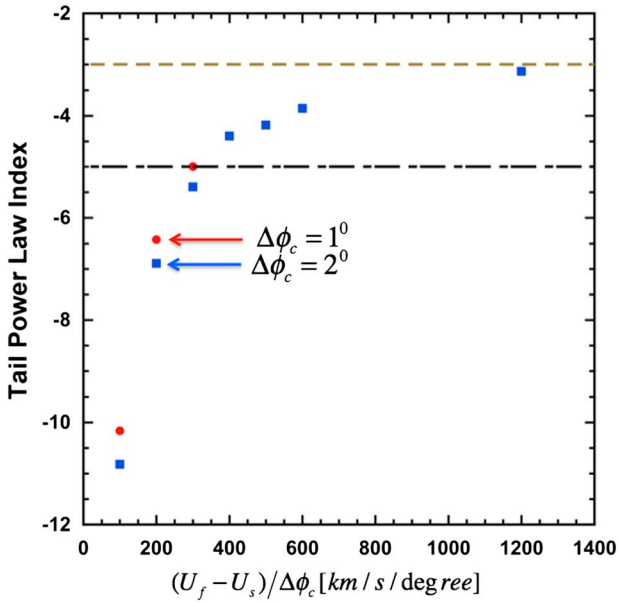

Figure 5. Power law index of the tail distribution, as simulated for various differences in the solar wind speed across the CIR. We also simulated two different widths of the solar wind speed transition $\Delta\phi_c$ ($\Delta\phi_c = 1^0$ in red and $\Delta\phi_c = 2^0$ in blue). The green and black dashed lines indicate -3 and -5 power law indices, respectively.

Figure 5 shows the power law index of the tail distribution for different parameters of the CIR. The power law index increases with $^{U_f} - U_s/_{\Delta}\phi_c$, and varies between -3 and steeper than -10. Without any additional acceleration terms in the transport equation, the acceleration is due to the gradual compression between the solar wind fast and slow stream. In this case, the -5 power law index is not a special solution, except that it represents an intermediate case in the range of parameters modeled. This circumstance motivates follow-up observational work to study the range of CIR compressions and the associated azimuthal velocity gradients, $^{U_f} - U_s/_{\Delta}\phi_c$, typically encountered in the solar wind at 1 AU and at other radial distances. Potentially, an observational relationship between these velocity gradients and the associated power law index of suprathermal particles could be established.

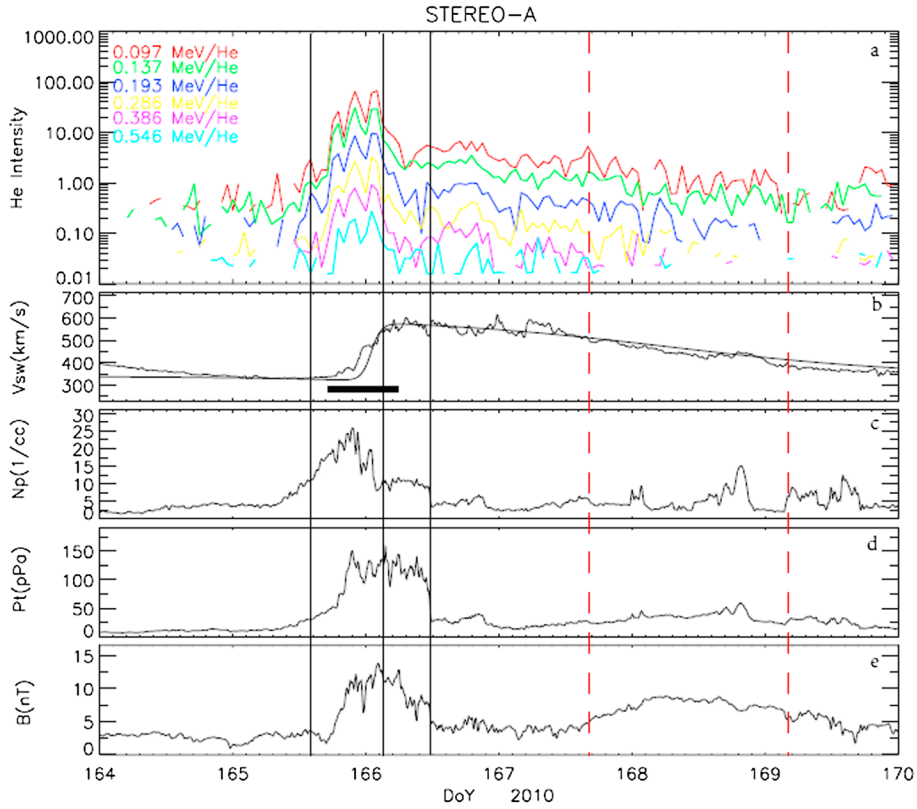

Figure 6. (a) One hour average energetic He intensity, which is interpreted as mostly He^+ from PUIs, as discussed in the text. (b–e) The 10 min average solar wind speed, density, proton total pressure, and magnetic field data. The black vertical lines mark the sector boundaries of the CIR, and the second vertical black line from the left is the stream interface. The red dashed vertical lines mark an interplanetary corona mass ejection.

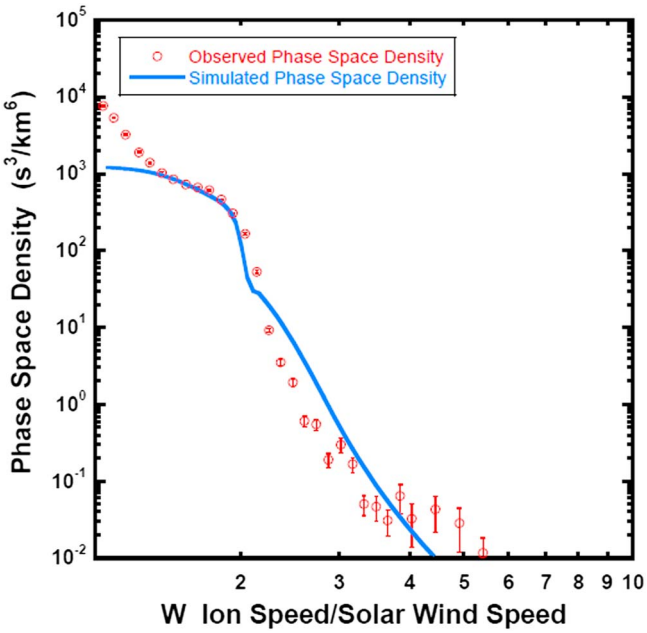

Figure 7. Comparison of predicted phase space density with observations plotted as a function of ion speed in the spacecraft frame divided by solar wind speed. The predicted phase space density is obtained by integrating the simulated PUI velocity distribution averaged in the CIR over the PLASTIC field-of-view and energy channels.

In the next example, we model the PUI velocity distributions for a CIR observed by STEREO-A, which occurred between 14 and 16 June (day of year 165–167), 2010 when the ecliptic longitude of STEREO-A is near 74^0 in the Heliocentric Earth Ecliptic (HEE) coordinate system. Figures 6a–6e shows the energetic He flux, solar wind speed, solar wind density, solar total pressure and magnetic field data for this CIR. Figure 6a shows 1 h average 0.097–0.546 Mev nucleon^{-1} He intensities measured by the Suprathermal Ion Telescope (SIT) [*Mason et al.,* 2008]. SIT is a time-of-flight mass spectrometer capable of identifying the elemental composition and measuring the intensity of heavy ions from ~30 keV/nucleon to 2 MeV/nucleon, but not the charge states. In the solar wind, the normal He^+/He^{++} ratio is on the order of 10^{-6}. However, extreme enhancement of the abundance ratio over the solar wind value with enhancement factors of $>10^3$ at suprathermal and high energies have been observed in CIRs [e.g., *Hilchenbach et al.,* 1999; *Chotoo et al.,* 2000; *Morris et al.,* 2001; *Möbius et al.,* 2002; *Kucharek et al.,* 2003]. These enhancements led to the suggestion that PUIs constitute an important source for further acceleration in CIRs. Therefore, the enhancement of the He flux in the CIR, as seen in Figure 6a, likely indicates local acceleration of interstellar He^+ PUIs. Figure 6b shows 10 min averaged solar wind speed measured by the Plasma and Suprathermal Ion Composition (PLASTIC) instrument [*Galvin et al.,* 2008]. The solid line is the solar wind speed used in the model. The bar in Figure 6b marks the time interval used for computing the PUI phase space density. Figures 6c–6e show the 10 min average solar wind density measured by PLASTIC, total proton pressure ($2n_pkT_p + B^2/\mu_0$), and interplanetary magnetic field strength measured by magnetometer [*Acuña et al.*, 2008] on STEREO-A. The solid vertical lines are the sector boundaries of the CIR and the stream interface. Parameters in the CIR model are $U_f = 600$ km/s, $U_s = 340$ km/s, $W = 200$ km/s, $\phi_c = 135^0$, $\phi_f = 105^0$, Δ_c, and $\Delta_f = 25^0$.

Figure 7 shows a comparison of predicted PUI phase space density with the observed PUI phase space density in the CIR from PLASTIC, which measures He^+ and He^{++} distributions from 0.4 to 80 keV separately. The predicted PUI phase space density is the PUI velocity distribution as obtained with EPREM using the same source function as in equation (17). It is averaged over the CIR and integrated over the PLASTIC field-of-view and energy channels. The increase in the observed phase space density at the lower energies may be attributed to a contribution of inner source ions, which completely dominate the pickup He^+ spectrum, and a potential contribution of heavy solar wind ions with mass per charge around 4. The predicted phase space density below the PUI cutoff speed [i.e., $1.4 \le W \le 2$] fits well. The phase space density above the cutoff speed appears qualitatively similar to the observations, but cannot be compared quantitatively. These results suggest that gradual compression of solar wind does play a role in the acceleration of particles to higher energy in CIRs.

5. Conclusions

We have used the EPREM kinetic code to model PUI propagation in a simplified CIR. In our simulation, we calculate the neutral gas spatial distribution with a hot interstellar gas model, taking into account solely photoionization. The newly created PUIs are injected as a ring distribution in velocity space according to

the local magnetic field direction. The PUI velocity distributions are obtained by solving the modified focused transport equation, where we ignored the transport perpendicular to the magnetic field and drift, and the stochastic acceleration. In summary, we have found the following:

1. In the undisturbed solar wind before the CIR compression region, the analytic solution of *Vasyliunas and Siscoe* [1976] agrees well with the distribution found with EPREM.
2. In the compression region of the CIR, the negative gradient of the solar wind speed leads to a weaker cooling for the core PUIs, while the cooling is stronger in the rarefaction region.
3. Also, a power law high-energy tail distribution above the PUI cutoff speed in the solar wind frame is found in the CIR compression region without the presence of a shock.
4. The power law index of the tail distribution increases with the velocity gradient in the compression region $^{U_f}\!/_{\Delta} - U_s/_{\Delta}\phi_c$ and varies between -3 and steeper than -10.

The first two results are consistent with the proposed explanation for the observation of a PUI cooling rate that varies with solar activity in the conclusion of *Chen et al.* [2013]. In fact, such variations of the solar wind expansion during the radial PUI transport may be the most important driver for the observed changes in the slope of the core PUI distribution.

We also demonstrate that gradual compression of the solar wind in the compression region can significantly accelerate PUIs at or inside 1 AU. This effect provides further evidence that local CIR compression plays an important role in the acceleration process. While the power law index of the suprathermal tail distribution in our simulations varies between about -3 and -10, a power law index near the center of this range or close to -5 is found for the high-energy tail (above 2 times the solar wind speed) distribution in the EPREM simulations for particular velocity gradients in the CIR. The power law above the injection speed of pickup ions is sensitive to the velocity gradient in CIRs, which motivates future observational studies to test whether a relationship between the power law index and the velocity gradient can be established. In one case study provided here, the observed velocity gradient produces an energy distribution above the pickup ion injection speed that agrees well with observations, which suggests that gradual compression may play an important role in the formation of the frequently observed superathermal tails.

Acknowledgments

This work was supported by the Sun-2-Ice project, NSF grant 1135432 to the University of New Hampshire, and the NASA C-SWEPA grant NNX13AI75G to the University of New Hampshire. Computations were performed on Trillian, a Cray XE6m-200 supercomputer at University of New Hampshire supported by the NSF MRI program under grant PHY-1229408. The energetic particle data are available at STEREO SIT Data Documentation (http://www.srl.caltech.edu/STEREO/docs/SIT_Level1.html). The STEREO PLASTIC solar wind plasma data are available at STEREO LEVEL2 SERVER (http://aten.igpp.ucla.edu/forms/stereo/level2_plasma_and_magnetic_field.html). The STEREO PUI data are available at http://fiji.sr.unh.edu/team/he_plus_team/.

Yuming Wang thanks two reviewers for their assistance in evaluating this paper.

References

Acuña, M. H., D. Curtis, J. L. Scheifele, C. T. Russell, P. Schroeder, A. Szabo, and J. G. Luhmann (2008), The STEREO/IMPACT magnetic field experiment, *Space Sci. Rev.*, *136*(1–4), 203–226.

Bzowski, M., et al. (2012), Neutral interstellar helium parameters based on IBEX-Lo observations and test particle calculations, *Astrophys. J. Suppl.*, *198*(2), 12, 27, doi:10.1088/0067-0049/198/2/12.

Bzowski, M., M. Kubiak, M. Hłond, J. Sokół, M. Banaszkiewicz, and M. Witte (2014), Neutral interstellar He parameters in front of the heliosphere 1994–2007, *Astron. Astrophys.*, *569*, A8.

Chalov, S. (2001), Shock drift acceleration of pickup protons at corotating interaction regions, *J. Geophys. Res.*, *106*(A9), 18,667–18,675, doi:10.1029/2000JA000442.

Chalov, S., and H. Fahr (1999), Signatures of the interplanetary helium cone reflected by pick-up ions, *Sol. Phys.*, *187*(1), 123–144.

Chen, J. H., P. Bochsler, E. Möbius, and G. Gloeckler (2014), Possible modification of the cooling index of interstellar helium pickup ions by electron impact ionization in the inner heliosphere, *J. Geophys. Res. Space Physics*, *119*, 7142–7150, doi:10.1002/2014JA020357.

Chen, J. H., E. Möbius, G. Gloeckler, P. Bochsler, M. Bzowski, P. A. Isenberg, and J. M. Sokół (2013), Observational study of the cooling behavior of interstellar helium pick up ions in the inner heliosphere, *J. Geophys. Res. Space Physics*, *118*, 3946–3953, doi:10.1002/jgra.50391.

Chollet, E., J. Giacalone, and R. Mewaldt (2010), Effects of interplanetary transport on derived energetic particle source strengths, *J. Geophys. Res.*, *115*, A06101, doi:10.1029/2009JA014877.

Chotoo, K., N. A. Schwadron, G. M. Mason, T. H. Zurbuchen, G. Gloeckler, A. Posner, L. A. Fisk, A. B. Galvin, D. C. Hamilton, and M. R. Collier (2000), The suprathermal seed population for corotating interaction region ions at 1 AU deduced from composition and spectra of H^+, He^{2+}, and He^+ observed on Wind, *J. Geophys. Res.*, *105*(A10), 23,107–23,122, doi:10.1029/1998JA000015.

Dayeh, M., M. Desai, K. Kozarev, N. Schwadron, L. Townsend, M. PourArsalan, C. Zeitlin, and R. Hatcher (2010), Modeling proton intensity gradients and radiation dose equivalents in the inner heliosphere using EMMREM: May 2003 solar events, *Space Weather*, *8*, S00E07, doi:10.1029/2009SW000566.

Desai, M., R. Marsden, T. Sanderson, D. Lario, E. Roelof, G. Simnett, J. Gosling, A. Balogh, and R. Forsyth (1999), Energy spectra of 50-keV to 20-MeV protons accelerated at corotating interaction regions at Ulysses, *J. Geophys. Res.*, *104*(A4), 6705–6719, doi:10.1029/1998JA900176.

Ebert, R. W., M. A. Dayeh, M. I. Desai, and G. M. Mason (2012), Corotating interaction region associated suprathermal helium ion enhancements at 1 AU: Evidence for local acceleration at the compression region trailing edge, *Astrophys. J.*, *749*(1).

Erdős, G. (1999), Scattering mean free path of energetic protons in the Heliosphere, Proceedings of the 26th International Cosmic Ray Conference, 6, 316.

Fahr, H. (1971), The interplanetary hydrogen cone and its solar cycle variations, *Astron. Astrophys.*, *14*, 263.

Fisk, L. A., and G. Gloeckler (2006), The common spectrum for accelerated ions in the quiet-time solar wind, *Astrophys. J.*, *640*(1), L79–L82.

Fisk, L. A., and G. Gloeckler (2007), Thermodynamic constraints on stochastic acceleration in compressional turbulence, *Proc. Natl. Acad. Sci. U.S.A.*, *104*(14), 5749–5754.

Fisk, L. A., and G. Gloeckler (2008), Acceleration of suprathermal tails in the solar wind, *Astrophys. J.*, *686*(2), 1466–1473.
Fisk, L. A., and M. A. Lee (1980), Shock acceleration of energetic particles in corotating interaction regions in the solar wind, *Astrophys. J.*, *237*(2), 620–626.
Galvin, A. B., et al. (2008), The Plasma and Suprathermal Ion Composition (PLASTIC) investigation on the STEREO observatories, *Space Sci. Rev.*, *136*(1–4), 437–486.
Geiss, J., G. Gloeckler, U. Mall, R. Vonsteiger, A. B. Galvin, and K. W. Ogilvie (1994), Interstellar oxygen, nitrogen and neon in the heliosphere, *Astron. Astrophys.*, *282*(3), 924–933.
Giacalone, J., J. R. Jokipii, and J. Kota (2002), Particle acceleration in solar wind compression regions, *Astrophys. J.*, *573*(2), 845–850.
Gloeckler, G. (2003), Ubiquitous suprathermal tails on the solar wind and pickup ion distributions, in Solar Wind Ten, *AIP Conf. Proc.*, *679*, 583–588.
Gloeckler, G., J. Geiss, H. Balsiger, L. A. Fisk, A. B. Galvin, F. M. Ipavich, K. W. Ogilvie, R. Vonsteiger, and B. Wilken (1993), Detection of interstellar pick-up hydrogen in the solar system, *Science*, *261*(5117), 70–73.
Gloeckler, G., et al. (2004), Observations of the helium focusing cone with pickup ions, *Astron. Astrophys.*, *426*(3), 845–854.
Hilchenbach, M., H. Grünwaldt, R. Kallenbach, B. Klecker, H. Kucharek, F. Ipavich, and A. Galvin (1999), Observation of suprathermal helium at 1 AU: Charge states in CIRs, in Solar Wind Nine, *AIP Conf. Proc.*, *471*, 605–608.
Hill, M. E., N. A. Schwadron, D. C. Hamilton, R. D. DiFabio, and R. K. Squier (2009), Interplanetary Suprathermal He+ and He++ observations during quiet periods from 1 to 9 AU and implications for particle acceleration, *Astrophys. J. Lett.*, *699*(1), L26–L30.
Isenberg, P. A. (1997), A hemispherical model of anisotropic interstellar pickup ions, *J. Geophys. Res.*, *102*(A3), 4719–4724, doi:10.1029/96JA03671.
Katushkina, O. A., V. V. Izmodenov, B. E. Wood, and D. McMullin (2014), Neutral interstellar helium parameters based on Ulysses/GAS and IBEX-Lo observations: What are the reasons for the differences?, *Astrophys. J.*, *789*(1), 80.
Kocharov, L., G. A. Kovaltsov, J. Torsti, A. Anttila, and T. Sahla (2003), Modeling the propagation of solar energetic particles in corotating compression regions of solar wind, *J. Geophys. Res.*, *108*(A11), 1404, doi:10.1029/2003JA009928.
Kolmogorov, A. N. (1941), Dissipation of energy in locally isotropic turbulence, *Dokl. Akad. Nauk SSSR*, *32*(1), 16–18.
Kóta, J. (2000), Diffusion of energetic particles in focusing fields, *J. Geophys. Res.*, *105*(A2), 2403–2411, doi:10.1029/1999JA900469.
Kóta, J., W. Manchester, and T. Gombosi (2005), SEP acceleration at realistic CMEs: Two sites of acceleration?, *Int. Cosmic Ray Conf.*, *1*, 125.
Kucharek, H., E. Möbius, W. Li, C. J. Farrugia, M. A. Popecki, A. B. Galvin, B. Klecker, M. Hilchenbach, and P. A. Bochsler (2003), On the source and acceleration of energetic He+: A long-term observation with ACE/SEPICA, *J. Geophys. Res.*, *108*(A10), 8040, doi:10.1029/2003JA009938.
Lallement, R., and J.-L. Bertaux (2014), On the decades-long stability of the interstellar wind through the solar system, *Astron. Astrophys.*, *565*, A41.
Leonard, T. W., et al. (2015), Revisiting the ISN flow parameters, using a variable IBEX pointing strategy, *Astrophys. J.*, *804*(1), 42, 6, doi:10.1088/0004-637X/804/1/42.
Mason, G. (2000), Composition and energy spectra of ions accelerated in corotating interaction regions, in ACE 2000 Symposium, *AIP Conf. Proc.*, *528*, 234–241.
Mason, G., A. Korth, P. Walpole, M. Desai, T. Von Rosenvinge, and S. Shuman (2008), The Suprathermal Ion Telescope (SIT) for the IMPACT/SEP investigation, *Space Sci. Rev.*, *136*(1–4), 257–284.
McComas, D. J., et al. (2015), Warmer local interstellar medium: A possible resolution of the Ulysses-IBEX enigma, *Astrophys. J.*, *801*(1), 28, 7, doi:10.1088/0004-637X/801/1/28.
Möbius, E., D. Hovestadt, B. Klecker, M. Scholer, G. Gloeckler, and F. M. Ipavich (1985), Direct observation of He+ pick-up ions of interstellar origin in the solar wind, *Nature*, *318*(6045), 426–429.
Möbius, E., B. Klecker, P. Bochsler, G. Gloeckler, H. Kucharek, K. Simunac, A. Galvin, L. Ellis, C. Farrugia, and L. Kistler (2010), He pickup ions in the inner heliosphere—Diagnostics of the local interstellar gas and of interplanetary conditions, in 9th Annual International Astrophysics Conference, *AIP Co nf. Proc.*, *1302*(1), 37–43.
Möbius, E., D. Morris, M. Popecki, B. Klecker, L. Kistler, and A. Galvin (2002), Charge states of energetic (≈0.5 MeV/n) ions in corotating interaction regions at 1 AU and implications on source populations, *Geophys. Res. Lett.*, *29*(2), 1016, doi:10.1029/2001GL013410.
Möbius, E., D. Rucinski, D. Hovestadt, and B. Klecker (1995), The helium parameters of the very local interstellar medium as derived from the distribution of He+ pickup Ions in the solar wind, *Astron. Astrophys.*, *304*(2), 505–519.
Möbius, E., et al. (2012), Interstellar gas flow parameters derived from interstellar boundary Explorer-Lo observations in 2009 and 2010: Analytical analysis, *Astrophys. J. Suppl.*, *198*(2), 11, 18, doi:10.1088/0067-0049/198/2/11.
Morris, D., E. Möbius, M. Lee, M. Popecki, B. Klecker, L. Kistler, and A. Galvin (2001), Implications for source populations of energetic ions in co-rotating interaction regions from ionic charge states, in A Joint Soho/ACE Workshop, *AIP Conf. Proc.*, *598*, 201–204.
Parker, E. N. (1965), Passage of energetic charged particles through interplanetary space, *Planet. Space Sci.*, *13*(1), 9–49.
Roelof, E. (1969), *Lectures in High Energy Astrophysics*, edited by H. Ögelman and J. R. Wayland, pp. 111–135, NASA.
Ruffolo, D. (1995), Effect of adiabatic deceleration on the focused transport of solar cosmic rays, *Astrophys. J.*, *442*(2), 861–874.
Sakai, T. (2002), Time profile of solar energetic particles fit using a mean free path considering the radial dependence of both magnetic field strength and fluctuations, *Earth Planets Space*, *54*(6), 727–732.
Schwadron, N. (1998), A model for pickup ion transport in the heliosphere in the limit of uniform hemispheric distributions, *J. Geophys. Res.*, *103*(A9), 20,643–20,649, doi:10.1029/98JA01686.
Schwadron, N., J. Geiss, L. Fisk, G. Gloeckler, T. H. Zurbuchen, and R. V. Steiger (2000), Inner source distributions: Theoretical interpretation, implications, and evidence for inner source protons, *J. Geophys. Res.*, *105*(A4), 7465–7472, doi:10.1029/1999JA000225.
Schwadron, N. A., et al. (2010), Earth-Moon-Mars Radiation Environment Module framework, *Space Weather*, *8*, S00E02, doi:10.1029/2009SW000523.
Skilling, J. (1971), Cosmic rays in galaxy—Convection or diffusion, *Astrophys. J.*, *170*(2), 265.
Thomas, G. E. (1978), The interstellar wind and its influence on the interplanetary environment, *Annu. Rev. Earth Planet. Sci.*, *6*, 173–204.
Vincent, F. E., et al. (2014), Observations of the interplanetary hydrogen Solar Cycle 23 and 24. What can we deduce about the local interstellar medium, *Astrophys. J. Lett.*, *788*(2), L25.
Vasyliunas, V. M., and G. L. Siscoe (1976), On the flux and energy spectrum of interstellar ions in solar system, *J. Geophys. Res.*, *81*(7), 1247–1252, doi:10.1029/JA081i007p01247.
Wu, F. M., and D. L. Judge (1979), Temperature and flow velocity of the interplanetary gases along solar radii, *Astrophys. J.*, *231*(2), 594–605.